Application of the Transition State Theory in the Study of the Osmotic Permeabilities of AQP7, AQP10 and GlpF

Ruth Chan and Liao Y. Chen *

Posted Date: 19 June 2025

doi: 10.20944/preprints202506.1617.v1

Keywords: aquaglyceroporin; osmotic permeability; transition state theory; molecular dynamics simulation

 doi:10.20944/preprints202506.1617.v1

Article

Application of the Transition State Theory in the Study of the Osmotic Permeabilities of AQP7, AQP10 and GlpF

Ruth Chan and Liao Y. Chen *

Department of Physics, The University of Texas at San Antonio, San Antonio, Texas 78249 USA

* Correspondence: liao.chen@utsa.edu

Abstract

Aquaglyceroporins, including human AQP7, AQP10, and *E. coli* GlpF, are known to facilitate movements of glycerol, water, and some other uncharged molecules across the cell membrane. In this study we focused on the transport of water molecules in the absence of glycerol for AQP7, AQP10 and GlpF using the Transition State Theory for the novel application of permeability and kinetics studies. We conducted around 500 ns of *in silico* simulations of the aquaglyceroporins embedded in lipid bilayer membranes with intracellular-extracellular asymmetries in leaflet lipid compositions. For the water permeability analysis, we computed the transition rate constant with correction for recrossing events where the water molecules do not completely traverse the protein channel from one side of the membrane to the other side. We also studied the hydrogen bond distributions of the single-file waters and channel residues and linear water densities along the pores of the aquaglyceroporins. Interestingly, we found that there was an inverse correlation between the number of single-file water molecules in the channel to osmotic permeability.

Keywords: aquaglyceroporin; osmotic permeability; transition state theory; molecular dynamics simulation

Introduction

Aquaporins (AQPs), a large family of integral membrane proteins, are found in humans and many other living organisms. They may be permeable to water exclusively (orthodox aquaporins), and some are also permeable to small uncharged solutes such as glycerol (aquaglyceroporins). AQPs play a vital role in osmoregulation which is essential to all life forms. Amongst the aquaglyceroporins, the crystal structure of the glycerol uptake facilitator protein (GlpF) from *Escherichia coli* (*E. coli*) had been long established [1], enabling extensive *in vitro* and theoretical-computational studies [2–16]. Conversely, the high-resolution crystal structures were more recently identified for AQP10 in 2018[17], and for AQP7 in 2020 [18,19]. Many previous studies on these 'newer' aquaglyceroporins AQP7 [18–26], and AQP10 [17,27–29], were thus largely *in vitro*.

Over the years, various computational models have been developed to study for, *e.g.*, transport kinetics of carrier and channel proteins at the atomic level and nanosecond timescale. Molecular dynamics simulations help complement the limitations of *in vitro* studies, thus enabling a greater overall understanding of these proteins essential to the life of the cells within the organism. Zhu *et al.* introduced the computational method utilizing the creation of a hydrostatic pressure gradient under periodic boundary conditions to observe the net water flow through the channels [30]. With a hydrostatic pressure difference established by subjecting the water molecules to a constant force, along with constraints and counter forces on the membrane/protein and elimination of the force on the water molecules inside the channel, the single channel osmotic permeability could be calculated from the retrieval of the single channel hydraulic permeability. At the time, computational power was limited with respect to today, and thus large pressure differences were required to yield results

 doi:10.20944/preprints202506.1617.v1

from shorter simulations. A later study related the concentration differences of the impermeant solute, ΔC_S (mol/cm^3) and water flux, j_W (mol/s) with the water chemical potential, $\Delta\mu$ (termed the collective diffusion model). This allowed the study of water movement in channels under equilibrium and non-equilibrium conditions by utilizing the development of a random walk approximation for the water molecules in the channel. With this model, calculating the osmotic permeability was equated to calculating the diffusion coefficient [31]. Subsequently, Wambo et al. proposed the method of computing water flux induced by a small NaCl osmolyte concentration gradient (in the mM range) across the membrane which yielded results with a greater level of accuracy. To increase the signal-to-noise ratio, a large model system was used with four tetramers embedded in a large patch of lipid bilayer representing the cellular membrane [3].

In 2020, our lab utilized the Transition State Theory (TST) for a novel application in the computation of osmotic permeabilities of AQP1 and AQP3 [32]. Developed in the 1930s by Eyring et al., the TST provides understanding of thermally activated processes through changes in the free-energy landscape along the reaction pathway. The TST method has been traditionally applied for example, in the study of chemical reactions and the unfolding of proteins and RNA structures. Expanding upon the TST fundamental dynamical assumption (or no-recrossing assumption), we introduced the correction factor κ to exclude events of water molecules recrossing the dividing plane. Considering the rugged potential energy landscape of the aquaporin channel, we set the dividing plane $z = z_0$ as the most constricted point in the aquaporin channel and evaluated κ by following every event trajectory of a molecule crossing the dividing plane from the intracellular (IC) side to the extracellular (EC) side until it either recrosses the plane back to the IC side or moves out of the channel into the EC bulk (or vice versa from EC to IC). The validity of our method was supported by the *in vitro* results from the well-established protocol of cell swelling/shrinkage studies using stopped-flow experiments on erythrocytes [32].

In this study, we further applied the TST method specifically for the study of aquaglyceroporins AQP7, AQP10, and GlpF for the computation of osmotic permeabilities at 5°C and 25°C. We excluded glycerol from the simulations as it has been previously shown that aquaglyceroporins have a high affinity for glycerol, which negatively affects osmotic permeability[5,18,33–36]. As will be detailed later in this paper, we found that the water permeability of AQP10 was the highest, followed by GlpF, and then AQP7. Interestingly, our results agreed with Horner *et al.* who found a direct correlation between the number of single-file water molecules in the channel to the permeability of water, through the calculation of single-channel osmotic permeability, p_f, with great accuracy from *in vitro* studies [4]. Previous experimental and computational results on GlpF also concurred with our findings [3,4], which confirmed the validity of our method. To further study the basis of the differences in permeability, we also examined the linear density of water in the channels, and the differences in the selectivity filter (sf) of these aquaglyceroporins.

Methods

Model System Setup and Simulation Parameters

CHARMM-GUI was used to set up the all-atom models of the GlpF, AQP7 and AQP10 tetramers which coordinates were taken from PDB ID 1FX8[1], 6QZI[18] and 6F7H[17] respectively. Each individual tetramer was embedded in a 117Å x 117Å patch of model membrane with the lipid compositions of 20% cholesterol (CHL1), 30% phosphocholine (POPC), and 49% phosphatidylethanolamine (POPE) for AQP7; 68% POPE, 27% phosphoglycerol (POPG), and 5% phosphocardiolipin (PMCL2) for GlpF; and 20% CHL1 and 80% POPE for AQP10 respectively (Figures 1–3). The positioning of the tetramers was determined by matching the hydrophobic side surface with the lipid tails and aligning the channel axes perpendicular to the membrane. The AQP-membrane complex was sandwiched between two layers of TIP3P waters, each of which was approximately 30Å thick. The system was then neutralized and salinated with Na^+ and Cl^- ions to a salt concentration of 150 mM. We employed NAMD 2.13[37] as the molecular dynamics (MD) engine

 doi:10.20944/preprints202506.1617.v1

and used CHARMM36 parameters[38–40] for inter-and intra-molecular interactions. After the initial equilibration steps, we fully equilibrated the system by running unbiased MD for 200 to 500 ns with constant pressure at 1.0 bar (Nose-Hoover barostat) and constant temperature at 278.15K and 298.15K (Langevin thermostat) respectively. The Langevin damping coefficient was chosen to be 1/ps. The period boundary conditions were applied to all three dimensions. The particle mesh Ewald (PME) was used for the long-range electrostatic interactions (grid level: 128 x 128 x 128). The time step was 2.0 fs. The cut-off for long-range interactions was set to 10Å with a switching distance of 9Å.

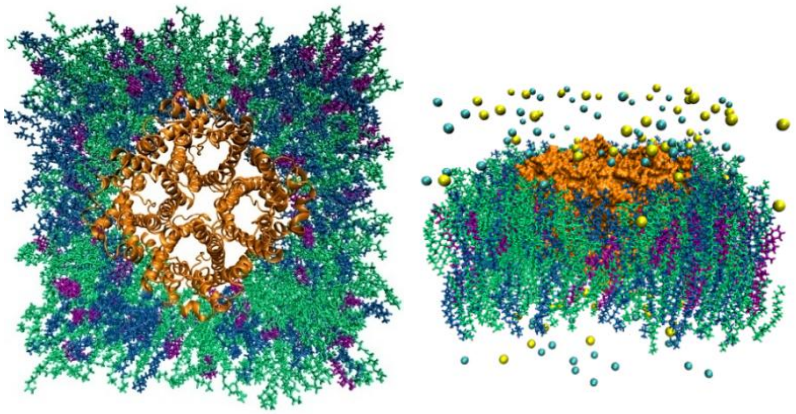

Figure 1. AQP7 model system. In the left panel is the top view from the EC side and, in the right panel is the side view. The protein tetramer is colored orange. The POPE lipids are indicated in green, CHL1 in purple, and POPC in dark blue. The Na+ ions and Cl- anions are shown as yellow and cyan spheres respectively. Water molecules are not shown for clearer views of all other constituents of the system.

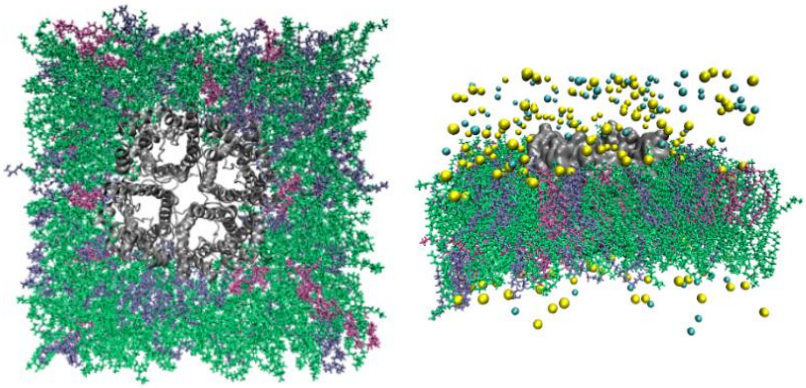

Figure 2. GlpF model system. In the left panel is the top view from the EC side, in the right panel, is the side view. The protein tetramer is in gray, and POPE lipids are indicated in green, PMCL2 in mauve, and POPG in ice blue. The Na+ ions and Cl- anions are shown as yellow and cyan spheres respectively. Water molecules are not shown for clearer views of all other constituents of the system.

 doi:10.20944/preprints202506.1617.v1

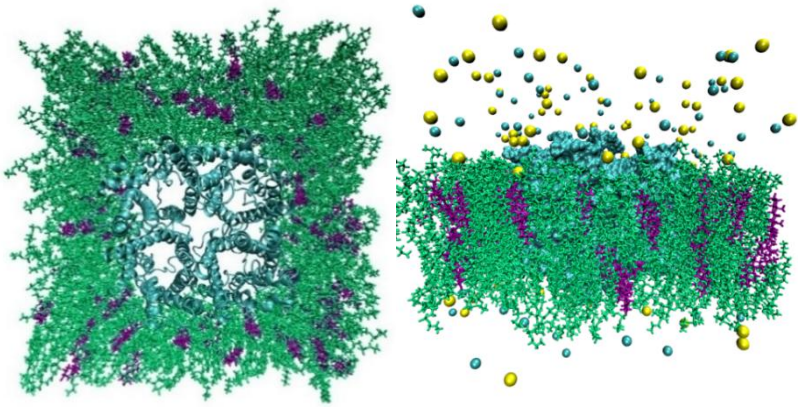

Figure 3. AQP10 model system. In left panel is the top view from the EC side and, in the right is the side view. The protein tetramer is in cyan, POPE lipids are indicated in green, and CHL1 in purple. The Na+ ions and Cl- anions are shown as yellow and cyan spheres respectively. Water molecules are not shown for clearer views of all other constituents of the system.

Transition State Theory for Calculation of Water Permeability

The permeability of water was calculated using the transition state theory with correction for recrossing events as detailed in Ref. [32]. Here we repeat the prescribed steps: An osmotic gradient is generated by an imbalance in impermeable osmolyte concentrations between two sides of a membrane. In the absence of hydraulic pressure difference, the intracellular (IC) to extracellular (EC) transition rate constant of water k_{ItoE} is related to the EC-to-IC rate constant k_{EtoI} as follows: $k_{ItoE} = k_{EtoI} exp[(c_e - c_i)v_W]$. The EC and IC concentrations of the impermeable solutes is denoted by c_e and c_i, respectively, and v_W is the molar volume of water. Under a hyperosmotic condition, $c_e - c_i > 0$, therefore $k_{ItoE} > k_{EtoI}$ and the outward chemical potential gradient induces a net efflux of water. The corresponding transition rate (transitions per unit time facilitated by one AQP channel) $r = k_{ItoE}(1/v_W - c_i) - k_{EtoI}(1/v_W - c_e)$. Note that $1/v_W$ is the concentration of water molecules in the absence of solutes. The presence of solutes reduces the water concentration. Furthermore, the validity of these formulas is limited to the dilute solution regime, namely, $(c_e - c_i)v_W \ll 1$, which is quantitatively accurate for osmolyte concentration in the sub Molar range. In this regime, the linear expansion in terms of $(c_e - c_i)$ is valid, which leads to the transition rate $r = 2k_0(c_e - c_e)$. Therefore, the water flux through a single AQP channel (the volume of water flowing through a channel per unit time), $J = rv_W/N_A = 2k_0(c_e - c_i)v_W/N_A$. Correspondingly, the single-channel permeability $p_f = J/(c_e - c_i) = 2k_0v_W/N_A$. Here k_0 is the rate constant $k_0 = k_{EtoI} = k_{ItoE}$ at equilibrium $(c_e = c_i)$ and N_A is the Avogadro number.

With the dividing plane between the IC and EC sides of z=0, only events of water molecules crossing the dividing plane in the positive z-direction and continuing onto the EC side (for IC-to-EC transitions, and vice versa for EC-to-IC transitions) without recrossing the dividing plane are considered. Therefore, in the application of the transition state theory (TST) this gives $k_0 = \kappa < v_z\delta(z - z_0) >_{v_z>0}$ where κ is the correction factor and $z = z_0 = 0$ is the dividing plane. The brackets indicate equilibrium statistical average of the velocity along the z-direction (or equivalently the negative z-direction for the EC-to-IC rate constant). Carrying out the equilibrium statistical average, we have $k_0 = \kappa\sqrt{RT/2\pi m_W n(z_0)}$ with m_W being the molar mass of water. The linear density of water at the dividing plane $n(z_0)$ can be readily evaluated with equilibrium sampling. The correction factor κ is equal to the number of successful transport events (ending up in the EC bulk at ($z > 15$) or IC bulk ($z < -15$)) divided by the total number of events of crossing the dividing plane. Water linear density along the z-axis was computed from scripts modified from Wang et al.[41]

 doi:10.20944/preprints202506.1617.v1

We also calculated the Arrhenius activation energy for the systems from the permeability values at 5°C and 25°C for the analysis of the effect temperature on the permeability of the protein channels. The Arrhenius activation energy, E_a was computed using the formula $E_a = \frac{RT_1 \ln\left(\frac{p_1}{p_2}\right)}{\frac{T_1}{T_2}-1}$, where R is the gas constant, T_1 and T_2 are the two temperatures in Kelvin, and p_1 and p_2 are the two corresponding permeabilities.

Results and Discussion

Single-Channel Osmotic Permeability, p_f, of AQP7, GlpF and AQP10

Following equilibration of the systems, as confirmed by RMSD analysis (Figure S1 in Supplementary Information), we ran the equilibrium MD for an additional 100 ns for each system counting the permeation events for the analysis of permeabilities. Using the TST method, the total number of permeation attempts by water molecules from both the EC and IC sides were computed over the equilibrated simulation length for all AQPs at 5°C and 25°C. The total number of successful events were also calculated (multiplied by 50 to allow the graph to be on the same scale) (left columns of Figures 4 and 5), with the correction for recrossing events. The success ratios (%), i.e. the κ values were obtained by dividing the total number of successful events of permeation by the total number of attempts. It can be seen at both temperatures that for GlpF and AQP10 there was a similar net transport of water molecules from one side of the membrane to the other, which was greater compared to AQP7 (right columns of Figures 4 and 5). As the κ values remained steady throughout the simulation duration, it can be inferred that the amount of water molecules successfully traversing the channel over time could be due to the inherent characteristics of the channels.

Permeability values of p_f were illustrated as a function of time in Figures 4 and 5, with the average values and error margins listed in Table 1. Upon examination, there is a consistent trend at both temperatures with the highest permeability seen for AQP10 (17.929 ± 0.028 at 25°C; 11.395 ± 0.028 at 5°C), followed by GlpF (15.304 ± 0.098 at 25°C; 9.657 ± 0.033 at 5°C), and then AQP7 (6.839 ± 0.047 at 25°C; 4.664 ± 0.019 at 5°C). Also, with the increase in temperature from 5°C to 25°C, as expected, osmotic permeability increased for all aquaglyceroporins due to the rise in thermal fluctuations. Existing osmotic permeability *in vitro* data for GlpF, AQP7 and AQP10 vary considerably over several orders of magnitude from 10^{-13}cm^3/s per channel. This is mainly due to the difficulty in determining the density of water channels from the various cellular/reconstituted systems to calculate single-channel transport rates from membrane permeability experimental assays. However, in a recent study by Horner et al., high-precision GlpF permeability values were found through rigorous experimental methods to measure the abundance of reconstituted aquaporins [4]. The experimentally derived permeability of GlpF to water at 5°C (11.7 x 10^{-13}cm^3/s)[4] was in good agreement with our results (9.66 x 10^{-13}cm^3/s), and similarly for the estimated value at 25°C calculated by Horner et al. from the known activation energy (19.0 x 10^{-13}cm^3/s) in comparison to our values (15.3 x 10^{-13}cm^3/s).

 doi:10.20944/preprints202506.1617.v1

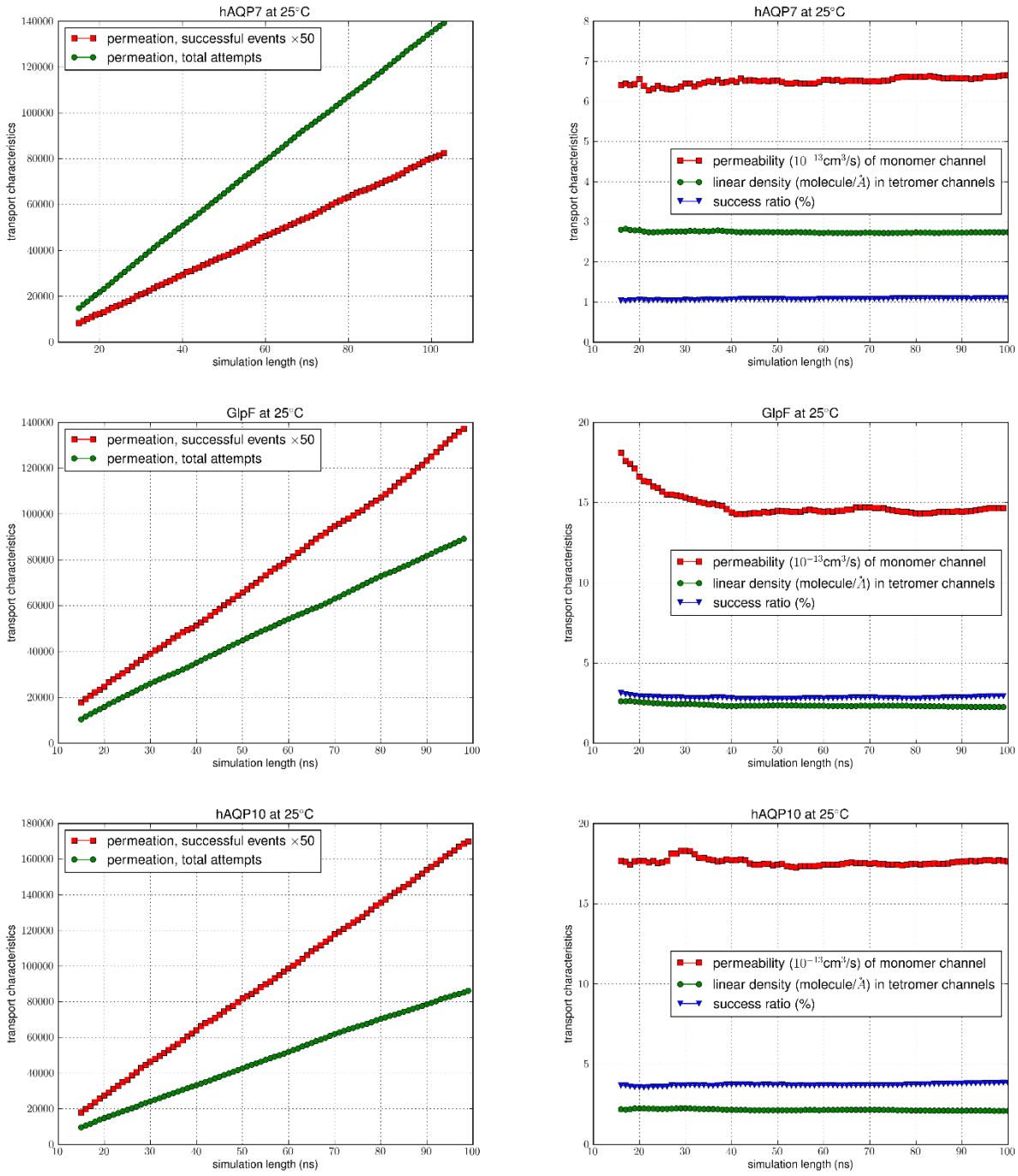

Figure 4. MD simulation results at 25°C. In the left columns, the number of successful events (x50) were compared to the total permeation attempts. Columns on the right indicate the permeability values, linear density and success ratio over the simulation length (100 ns).

 doi:10.20944/preprints202506.1617.v1

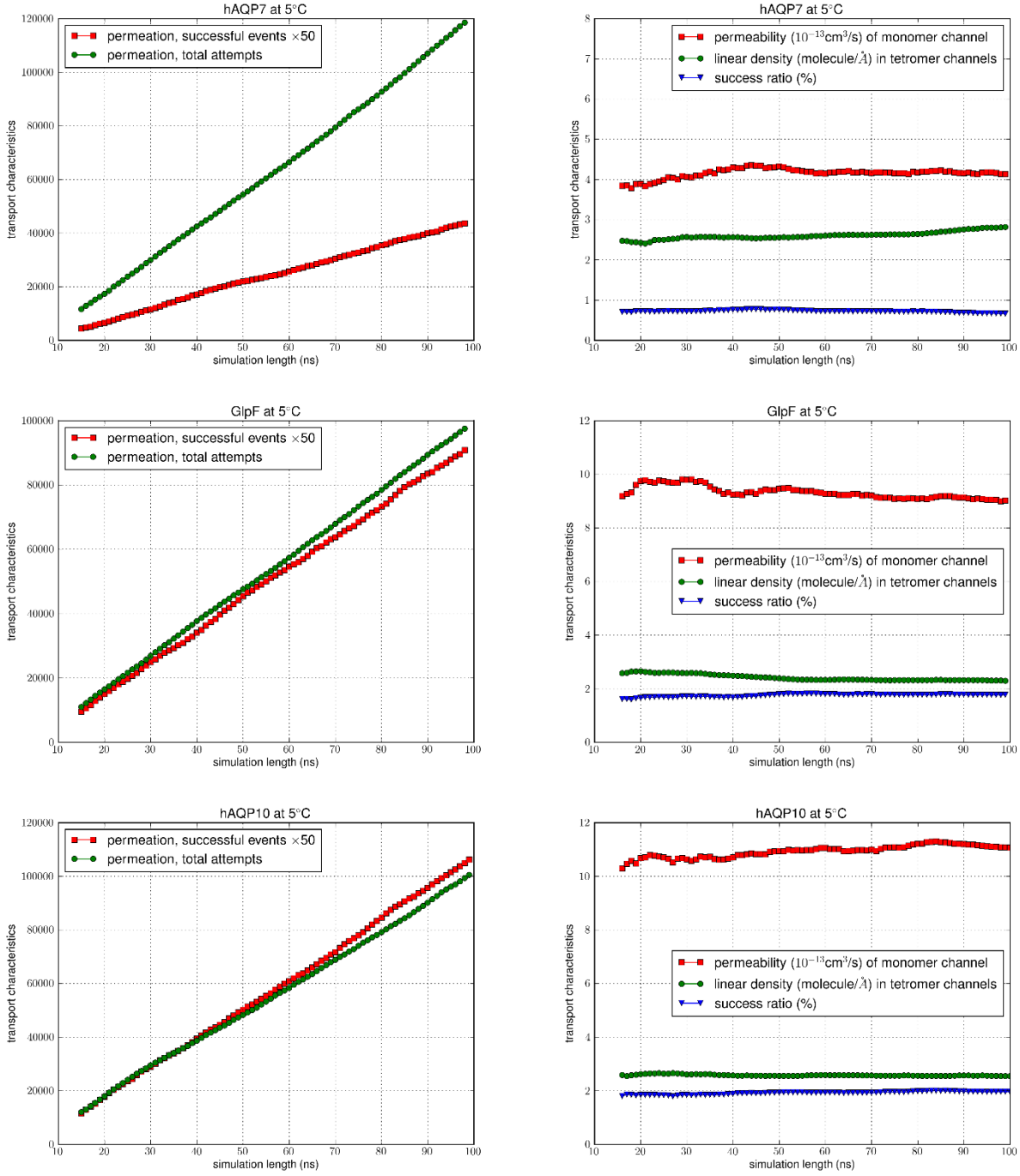

Figure 5. MD simulation results at 5°C. In the left columns, the number of successful events (x50) were compared to the total permeation attempts. Columns on the right indicate the permeability values, linear density and success ratio over the simulation length (100 ns).

Effect of Temperature on Osmotic Permeability

The Arrhenius activation barrier or energy for water permeation by all three aquaglyceroporins was remarkably similar at approximately 3.7 – 3.8 kcal/mol for GlpF and AQP10 and 3.2 kcal/mol for AQP7 for the simulations that were done in the absence of glycerol (Table 1). This is in line with experimental values for AQP7 [22] and GlpF [4] and in general indicates water movement through aqueous pores [42]. With glycerol present in the experiment, it has been reported that for GlpF the E_a value is 7 kcal/mol [12], showing that bound glycerol in the channel occludes other water or glycerol molecules from traversing it.

 doi:10.20944/preprints202506.1617.v1

We also looked at the RMSF values of the NPA motifs and the aromatic/arginine (ar/R) selectivity filter residues respectively and found that they were not significantly different between the studied aquaglyceroporins and between the two temperatures (Supp. Info Table S1). The values indicated that the average fluctuations of the amino acids in these regions (including the backbone and side chain) remained relatively stable throughout the simulation. This corroborated with the findings from the E_a values that the aquaglyceroporin water permeabilities were less dependent on temperature changes.

Table 1. Single-channel permeabilities p_f ($10^{-13}cm^3/s$) and Arrhenius activation energy, E_a (kcal/mol) of GlpF, AQP7 and AQP10.

AQP	p_f **($10^{-13}cm^3/s$) at 5°C**	p_f **($10^{-13}cm^3/s$) at 25°C**	E_a ***(kcal/mol)***
AQP7	4.664 ± 0.019	6.839 ± 0.047	3.154
GlpF	9.657 ± 0.033	15.304 ± 0.098	3.794
AQP10	11.395 ± 0.028	17.929 ± 0.028	3.734

Correlation Between Osmotic Permeability and Water-Protein Hydrogen Bonds

Figure 6 depicts the probability histograms of the hydrogen bonds between single-file water molecules in the channels (in blue) and between the water molecules and pore-lining residues for all three aquaglyceroporins (in orange) at 25°C. These values were averaged across the monomers (values for individual monomers are in Suppl. Info Figure S3 – S5 for 25°C, and S6 – S8 for 5°C). Also shown are the diagrams of single-file waters in the respective channels. The approximate number of water-protein hydrogen bonds were ~6.5 for AQP7 followed by ~5.5 for GlpF, and ~5.0 for AQP10 at both 25°C (Figure 6) and 5°C (Suppl. Info Figure S2). For all three aquaglyceroporins, the number of water-water hydrogen bonds was consistently lower than the water-protein hydrogen bonds, i.e. ~4.5 for AQP7, followed by ~4 for GlpF and ~3.5 for AQP10. Interestingly, the number of hydrogen-bonds between the single-file waters and channel residues inversely correlated with the permeability values of AQP7, GlpF and AQP10, i.e. increasing hydrogen bonds (or single-file waters) decreases aquaglyceroporin osmotic permeability. For AQP10, the reduced interaction of water molecules with the channel residues coupled with the widened channel radius may have contributed to the increased permeability. Additionally, amongst the aquaglyceroporins studied, AQP10 has the shortest region of single-file waters with most of the water molecules in the channel in a more compacted and bulk-like state. Single-file waters act as a rate-limiting step, preventing water molecules from overtaking each other and only permitting a single-direction water flow at any instance. Similarly, other studies have found that water permeability is influenced by the interactions between water and the pore-lining residues[43,44], and notably Horner et al. found that p_f increased exponentially with a decreasing number of hydrogen bond donating or accepting residues in the channel wall[4,45].

 doi:10.20944/preprints202506.1617.v1

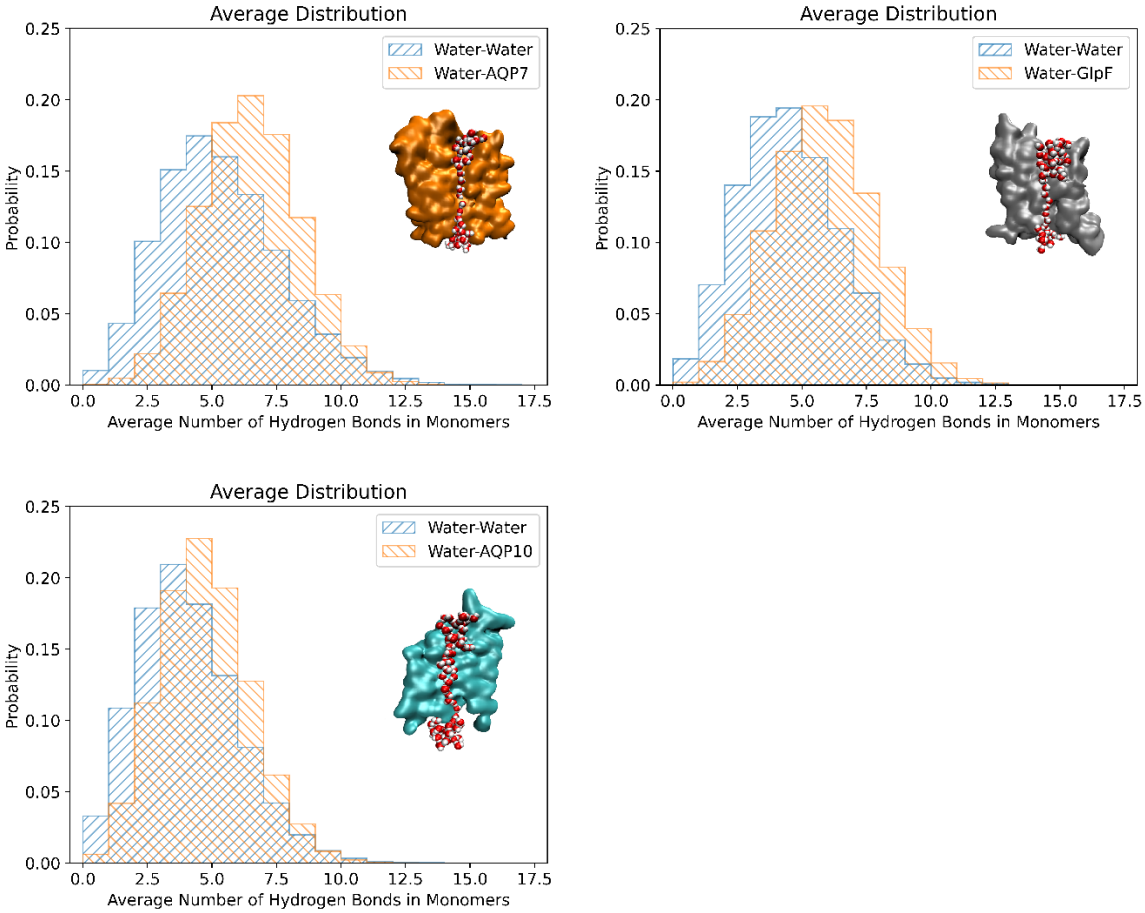

Figure 6. The number of hydrogen bonds formed (i) amongst the single-file waters in the channel (in blue) and (ii) between the single-file waters and pore-lining residues (in orange) of AQP7, GlpF and AQP10 respectively at 25°C. The results shown were averaged across all the monomers in the tetramer, and throughout the equilibrated simulation duration.

Effect of Channel Structure on Osmotic Permeability

To visualize the channel shape and dimensions in terms of how many water molecules can compact within a single channel, we calculated the water linear density values along and normal to the z-axis (Figure 7). This provided a representative depiction of the average channel capacity for water molecules throughout the simulation length upon equilibration. Higher density values indicate a smaller distance between the molecules (i.e. greater water packing) and a greater degree of disorder. Conversely, lower density values indicate that the water molecules are spaced further apart and are thus closer to the single-file configuration. As expected, the z-axis regions with low density values (≤ 2.5 molecule/nm^3) were the shortest for AQP10 (~ 10Å), followed by GlpF (~12 Å), and then AQP7 (~14Å) (Figure 7). At both the intracellular and extracellular openings the linear density increases at a rapid rate, eventually plateauing at the ends of the channels in contact with the bulk water region. Interestingly, for AQP10 there was a significant reduction in linear densities at 25°C compared to 5°C, which was not observed in AQP7 or GlpF. This corroborates with the greater difference in permeability values for AQP10 at the two temperatures compared with the other aquaglyceroporins. Moreover, a constriction in the channel opening at the intracellular side can be clearly seen for AQP10 from the linear density graphs, as was also found by Gotfryd et al.[17]

 doi:10.20944/preprints202506.1617.v1

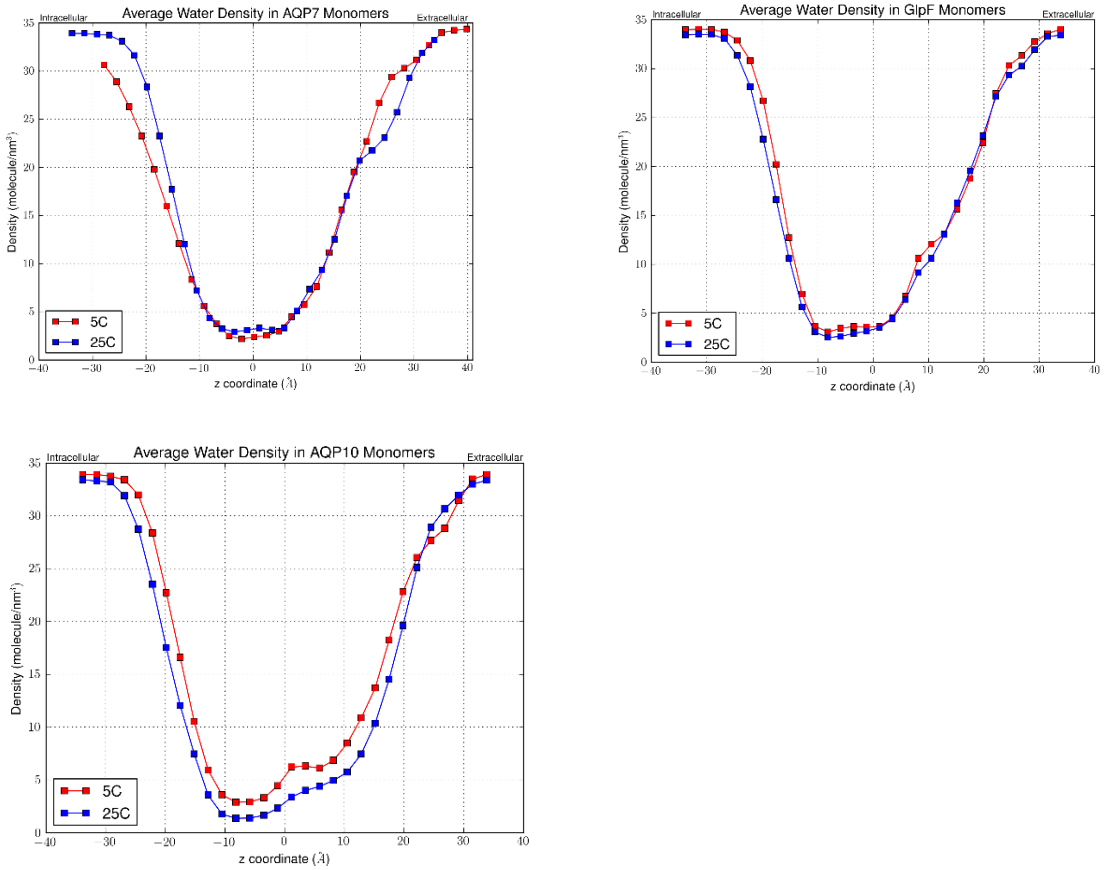

Figure 7. Linear density of water molecules in AQP7, GlpF and AQP10 channels respectively at 25°C and 5°C. Figures were averaged over the four monomers of each tetramer.

To further investigate the possible factors influencing permeability, we compared the selectivity filter (sf) regions of the three aquaglyceroporins, focusing on AQP7 and AQP10 in comparison with GlpF. Figure 8(a) depicts the sf of AQP10 which was considerably wider compared to AQP7 (sf residues indicated in yellow). The relatively open configuration of the AQP10 sf allows multiple water molecules to pass through simultaneously. Conversely, the AQP7 sf was significantly narrower and only allowed passage of water molecules from the EC side in single-file. Upon comparison of the AQP7 and AQP10 sf residues with GlpF, there were some significant differences in the configuration (Figure 8(b)). GlpF residues which contributed to the restriction site are W48, F200 and R206, whereas G191 is typically omitted from sf diagrams as it is located further away from the channel lining. Similarly, G202 from AQP10 is also situated away from the channel pore. AQP7 however was notably different, with G222 directly bonded to Y223, and thus possibly contributing to the decreased osmotic permeability due to the steric hindrance. The G222 residue of AQP7 on the EC side of the sf was almost parallel to the direction of water flow, causing a narrowing of the channel opening near the pore entrance. A closer examination of the superimposition of the sf residues of the aquaglyceroporins clearly showed that the AQP10 sf was significantly wider, as it lacked the characteristic aromatic residues (which restricts the molecules passing through) as found in GlpF and AQP7. Instead, for AQP10 these residues were replaced by smaller hydrophobic amino acids G62 and I211 (Figure 8(b)).

 doi:10.20944/preprints202506.1617.v1

Figure 8. Selectivity filter (sf) and NPA motifs. (a) The monomer AQP10 (cyan) is depicted with the sf in yellow and NPA motif in blue. The AQP7 monomer (orange) is included for comparison. (b) Sf residues; AQP10 is shown in cyan, AQP7 in orange, and GlpF in gray.

Conclusion

Through MD simulations using the established parameters, we measured the osmotic permeabilities of AQP7, AQP10 and GlpF with the novel application of the TST method. Our results were in agreement with recent experimental studies. From the analysis of the number of hydrogen bonds, linear densities and the selectivity filter, we obtained further insights into the probable factors contributing to the differences in permeabilities between these aquaglyceroporins. Notably, we found that there was an inverse correlation between the number of single-file water molecules in the channel to osmotic permeability.

Supplementary Information: The supplemental material contains tables and figures that are discussed but not included in the main paper.

Author contributions: RC wrote the paper. All participated in conducting the research and editing the manuscript.

Grant support: This work was supported by the NIH (GM121275).

Data availability: The Dataset (parameters, coordinates, scripts, *etc.*) to replicate this study will be available upon reasonable requests.

Acknowledgements: The authors acknowledge the computing resources provided by the Texas Advanced Computing Center (TACC) at the University of Texas at Austin.

Declaration: There are no conflicts to declare.

References

1. D. Fu *Et Al.*, "Structure Of A Glycerol-Conducting Channel And The Basis For Its Selectivity," (In Eng), *Science,* Vol. 290, No. 5491, Pp. 481-6, Oct 20 2000, Doi: 10.1126/Science.290.5491.481.
2. B. L. De Groot And H. Grubmüller, "Water Permeation Across Biological Membranes: Mechanism And Dynamics Of Aquaporin-1 And Glpf," *Science,* Vol. 294, No. 5550, Pp. 2353-2357, 2001, Doi: 10.1126/Science.1066115.
3. T. O. Wambo, R. A. Rodriguez, And L. Y. Chen, "Computing Osmotic Permeabilities Of Aquaporins Aqp4, Aqp5, And Glpf From Near-Equilibrium Simulations," (In Eng), *Biochimica Et Biophysica Acta. Biomembranes,* Vol. 1859, No. 8, Pp. 1310-1316, Aug 2017, Doi: 10.1016/J.Bbamem.2017.04.022.
4. A. Horner *Et Al.*, "The Mobility Of Single-File Water Molecules Is Governed By The Number Of H-Bonds They May Form With Channel-Lining Residues," *Science Advances,* Vol. 1, No. 2, P. E1400083, 2015, Doi: 10.1126/Sciadv.1400083.

 doi:10.20944/preprints202506.1617.v1

5. L. Y. Chen, "Glycerol Modulates Water Permeation Through Escherichia Coli Aquaglyceroporin Glpf," (In Eng), *Biochimica Et Biophysica Acta,* Vol. 1828, No. 8, Pp. 1786-93, Aug 2013, Doi: 10.1016/J.Bbamem.2013.03.008.
6. C. Aponte-Santamaría, J. S. Hub, And B. L. De Groot, "Dynamics And Energetics Of Solute Permeation Through The Plasmodium Falciparum Aquaglyceroporin," *Physical Chemistry Chemical Physics,* 10.1039/C004384m Vol. 12, No. 35, Pp. 10246-10254, 2010, Doi: 10.1039/C004384m.
7. M. Jensen And O. G. Mouritsen, "Single-Channel Water Permeabilities Of Escherichia Coli Aquaporins Aqpz And Glpf," (In Eng), *Biophys J,* Vol. 90, No. 7, Pp. 2270-84, Apr 1 2006, Doi: 10.1529/Biophysj.105.073965.
8. J. K. Lee, S. Khademi, W. Harries, D. Savage, L. Miercke, And R. M. Stroud, "Water And Glycerol Permeation Through The Glycerol Channel Glpf And The Aquaporin Family," *Journal Of Synchrotron Radiation,* Vol. 11, No. 1, Pp. 86-88, 2004, Doi: Https://Doi.Org/10.1107/S0909049503023872.
9. D. Lu, P. Grayson, And K. Schulten, "Glycerol Conductance And Physical Asymmetry Of The Escherichia Coli Glycerol Facilitator Glpf," (In Eng), *Biophys J,* Vol. 85, No. 5, Pp. 2977-87, Nov 2003, Doi: 10.1016/S0006-3495(03)74718-3.
10. E. Tajkhorshid *Et Al.*, "Control Of The Selectivity Of The Aquaporin Water Channel Family By Global Orientational Tuning," *Science,* Vol. 296, No. 5567, Pp. 525-530, 2002, Doi: 10.1126/Science.1067778.
11. M. Jensen, S. Park, E. Tajkhorshid, And K. Schulten, "Energetics Of Glycerol Conduction Through Aquaglyceroporin Glpf," (In Eng), *Proceedings Of The National Academy Of Sciences Of The United States Of America,* Vol. 99, No. 10, Pp. 6731-6, May 14 2002, Doi: 10.1073/Pnas.102649299.
12. M. J. Borgnia And P. Agre, "Reconstitution And Functional Comparison Of Purified Glpf And Aqpz, The Glycerol And Water Channels From <Em>Escherichia Coli</Em>," *Proceedings Of The National Academy Of Sciences,* Vol. 98, No. 5, Pp. 2888-2893, 2001, Doi: 10.1073/Pnas.051628098.
13. C. Maurel, J. Reizer, J. I. Schroeder, M. J. Chrispeels, And M. H. Saier, Jr., "Functional Characterization Of The Escherichia Coli Glycerol Facilitator, Glpf, In Xenopus Oocytes," (In Eng), *The Journal Of Biological Chemistry,* Vol. 269, No. 16, Pp. 11869-72, Apr 22 1994.
14. K. B. Heller, E. C. Lin, And T. H. Wilson, "Substrate Specificity And Transport Properties Of The Glycerol Facilitator Of Escherichia Coli," (In Eng), *Journal Of Bacteriology,* Vol. 144, No. 1, Pp. 274-8, Oct 1980, Doi: 10.1128/Jb.144.1.274-278.1980.
15. M. Hashido, M. Ikeguchi, And A. Kidera, "Comparative Simulations Of Aquaporin Family: Aqp1, Aqpz, Aqp0 And Glpf," (In Eng), *Febs Letters,* Vol. 579, No. 25, Pp. 5549-52, Oct 24 2005, Doi: 10.1016/J.Febslet.2005.09.018.
16. M. Ø. Jensen, E. Tajkhorshid, And K. Schulten, "Electrostatic Tuning Of Permeation And Selectivity In Aquaporin Water Channels," (In Eng), *Biophysical Journal,* Vol. 85, No. 5, Pp. 2884-2899, 2003/11// 2003, Doi: 10.1016/S0006-3495(03)74711-0.
17. K. Gotfryd *Et Al.*, "Human Adipose Glycerol Flux Is Regulated By A Ph Gate In Aqp10," (In Eng), *Nature Communications,* Vol. 9, No. 1, P. 4749, Nov 12 2018, Doi: 10.1038/S41467-018-07176-Z.
18. S. W. De Maré, R. Venskutonytė, S. Eltschkner, B. L. De Groot, And K. Lindkvist-Petersson, "Structural Basis For Glycerol Efflux And Selectivity Of Human Aquaporin 7," *Structure,* Vol. 28, No. 2, Pp. 215-222.E3, 2020/02/04/ 2020, Doi: Https://Doi.Org/10.1016/J.Str.2019.11.011.
19. F. J. Moss *Et Al.*, "Aquaporin-7: A Dynamic Aquaglyceroporin With Greater Water And Glycerol Permeability Than Its Bacterial Homolog Glpf," (In English), *Frontiers In Physiology,* Original Research Vol. 11, No. 728, 2020-June-30 2020, Doi: 10.3389/Fphys.2020.00728.
20. J. D. R. Schmidt, P. Walloch, B. Höger, And E. Beitz, "Aquaporins With Lactate/Lactic Acid Permeability At Physiological Ph Conditions," *Biochimie,* 2021/02/10/ 2021, Doi: Https://Doi.Org/10.1016/J.Biochi.2021.01.018.
21. A. Madeira, M. Camps, A. Zorzano, T. F. Moura, And G. Soveral, "Biophysical Assessment Of Human Aquaporin-7 As A Water And Glycerol Channel In 3t3-L1 Adipocytes," *Plos One,* Vol. 8, No. 12, P. E83442, 2013, Doi: 10.1371/Journal.Pone.0083442.

22. K. Ishibashi *Et Al.*, "Cloning And Functional Expression Of A New Water Channel Abundantly Expressed In The Testis Permeable To Water, Glycerol, And Urea," (In Eng), *The Journal Of Biological Chemistry,* Vol. 272, No. 33, Pp. 20782-6, Aug 15 1997, Doi: 10.1074/Jbc.272.33.20782.
23. T. Katano, Y. Ito, K. Ohta, T. Yasujima, K. Inoue, And H. Yuasa, "Functional Characteristics Of Aquaporin 7 As A Facilitative Glycerol Carrier," *Drug Metabolism And Pharmacokinetics,* Vol. 29, No. 3, Pp. 244-248, 2014/01/01/ 2014, Doi: Https://Doi.Org/10.2133/Dmpk.Dmpk-13-Rg-121.
24. M. Hara-Chikuma *Et Al.*, "Progressive Adipocyte Hypertrophy In Aquaporin-7-Deficient Mice: Adipocyte Glycerol Permeability As A Novel Regulator Of Fat Accumulation," (In Eng), *The Journal Of Biological Chemistry,* Vol. 280, No. 16, Pp. 15493-6, Apr 22 2005, Doi: 10.1074/Jbc.C500028200.
25. T. Hibuse *Et Al.*, "The Heart Requires Glycerol As An Energy Substrate Through Aquaporin 7, A Glycerol Facilitator," (In Eng), *Cardiovasc Res,* Vol. 83, No. 1, Pp. 34-41, Jul 1 2009, Doi: 10.1093/Cvr/Cvp095.
26. A. F. Mósca *Et Al.*, "Molecular Basis Of Aquaporin-7 Permeability Regulation By Ph," (In Eng), *Cells,* Vol. 7, No. 11, Nov 10 2018, Doi: 10.3390/Cells7110207.
27. K. Ishibashi, T. Morinaga, M. Kuwahara, S. Sasaki, And M. Imai, "Cloning And Identification Of A New Member Of Water Channel (Aqp10) As An Aquaglyceroporin," *Biochimica Et Biophysica Acta (Bba) - Gene Structure And Expression,* Vol. 1576, No. 3, Pp. 335-340, 2002/07/19/ 2002, Doi: Https://Doi.Org/10.1016/S0167-4781(02)00393-7.
28. S. Hatakeyama *Et Al.*, "Cloning Of A New Aquaporin (Aqp10) Abundantly Expressed In Duodenum And Jejunum," *Biochemical And Biophysical Research Communications,* Vol. 287, No. 4, Pp. 814-819, 2001/10/05/ 2001, Doi: Https://Doi.Org/10.1006/Bbrc.2001.5661.
29. M. Ishii *Et Al.*, "Dual Functional Characteristic Of Human Aquaporin 10 For Solute Transport," *Cellular Physiology And Biochemistry,* Vol. 27, No. 6, Pp. 749-756, 2011, Doi: 10.1159/000330083.
30. F. Zhu, E. Tajkhorshid, And K. Schulten, "Pressure-Induced Water Transport In Membrane Channels Studied By Molecular Dynamics," *Biophysical Journal,* Vol. 83, No. 1, Pp. 154-160, 2002/07/01/ 2002, Doi: Https://Doi.Org/10.1016/S0006-3495(02)75157-6.
31. F. Zhu, E. Tajkhorshid, And K. Schulten, "Collective Diffusion Model For Water Permeation Through Microscopic Channels," *Physical Review Letters,* Vol. 93, No. 22, P. 224501, 11/24/ 2004, Doi: 10.1103/Physrevlett.93.224501.
32. R. Chan, M. Falato, H. Liang, And L. Y. Chen, "In Silico Simulations Of Erythrocyte Aquaporins With Quantitative In Vitro Validation," (In Eng), *Rsc Advances,* Vol. 10, No. 36, Pp. 21283-21291, 2020, Doi: 10.1039/D0ra03456h.
33. R. A. Rodriguez, H. Liang, L. Y. Chen, G. Plascencia-Villa, And G. Perry, "Single-Channel Permeability And Glycerol Affinity Of Human Aquaglyceroporin Aqp3," (In Eng), *Biochimica Et Biophysica Acta. Biomembranes,* Vol. 1861, No. 4, Pp. 768-775, Apr 1 2019, Doi: 10.1016/J.Bbamem.2019.01.008.
34. R. A. Rodriguez, R. Chan, H. Liang, And L. Y. Chen, "Quantitative Study Of Unsaturated Transport Of Glycerol Through Aquaglyceroporin That Has High Affinity For Glycerol," (In Eng), *Rsc Advances,* Vol. 10, No. 56, Pp. 34203-34214, 2020, Doi: 10.1039/D0ra05262k.
35. L. Y. Chen, "Free-Energy Landscape Of Glycerol Permeation Through Aquaglyceroporin Glpf Determined From Steered Molecular Dynamics Simulations," (In Eng), *Biophysical Chemistry,* Vol. 151, No. 3, Pp. 178-80, Oct 2010, Doi: 10.1016/J.Bpc.2010.05.014.
36. L. Y. Chen, "Glycerol Inhibits Water Permeation Through Plasmodium Falciparum Aquaglyceroporin," (In Eng), *Journal Of Structural Biology,* Vol. 181, No. 1, Pp. 71-6, Jan 2013, Doi: 10.1016/J.Jsb.2012.10.007.
37. J. C. Phillips *Et Al.*, "Scalable Molecular Dynamics With Namd," (In Eng), *Journal Of Computational Chemistry,* Vol. 26, No. 16, Pp. 1781-802, Dec 2005, Doi: 10.1002/Jcc.20289.
38. R. B. Best *Et Al.*, "Optimization Of The Additive Charmm All-Atom Protein Force Field Targeting Improved Sampling Of The Backbone Φ, Ψ And Side-Chain X(1) And X(2) Dihedral Angles," (In Eng), *Journal Of Chemical Theory And Computation,* Vol. 8, No. 9, Pp. 3257-3273, Sep 11 2012, Doi: 10.1021/Ct300400x.
39. K. Vanommeslaeghe *Et Al.*, "Charmm General Force Field: A Force Field For Drug-Like Molecules Compatible With The Charmm All-Atom Additive Biological Force Fields," (In Eng), *Journal Of Computational Chemistry,* Vol. 31, No. 4, Pp. 671-90, Mar 2010, Doi: 10.1002/Jcc.21367.

 doi:10.20944/preprints202506.1617.v1

40. J. B. Klauda *Et Al.*, "Update Of The Charmm All-Atom Additive Force Field For Lipids: Validation On Six Lipid Types," (In Eng), *The Journal Of Physical Chemistry. B,* Vol. 114, No. 23, Pp. 7830-43, Jun 17 2010, Doi: 10.1021/Jp101759q.
41. Y. Wang, A. Kiziltas, P. Blanchard, And T. R. Walsh, "Calculation Of 1d And 2d Densities In Vmd: A Flexible And Easy-To-Use Code," *Computer Physics Communications,* Vol. 266, P. 108032, 2021/09/01/ 2021, Doi: Https://Doi.Org/10.1016/J.Cpc.2021.108032.
42. A. S. Verkman *Et Al.*, "Water Transport Across Mammalian Cell Membranes," *American Journal Of Physiology-Cell Physiology,* Vol. 270, No. 1, Pp. C12-C30, 1996, Doi: 10.1152/Ajpcell.1996.270.1.C12.
43. A. Hardiagon *Et Al.*, "Molecular Dynamics Simulations Reveal Statistics And Microscopic Mechanisms Of Water Permeation In Membrane-Embedded Artificial Water Channel Nanoconstructs," *The Journal Of Chemical Physics,* Vol. 154, No. 18, P. 184102, 2021, Doi: 10.1063/5.0044360.
44. D. Wragg, A. De Almeida, A. Casini, And S. Leoni, "Unveiling The Mechanisms Of Aquaglyceroporin-3 Water And Glycerol Permeation By Metadynamics," *Chemistry – A European Journal,* Vol. 25, No. 37, Pp. 8713-8718, 2019, Doi: Https://Doi.Org/10.1002/Chem.201902121.
45. A. Horner And P. Pohl, "Single-File Transport Of Water Through Membrane Channels," *Faraday Discuss.*, 10.1039/C8fd00122g Vol. 209, No. 0, Pp. 9-33, 2018, Doi: 10.1039/C8fd00122g.